Supporting Information

Boosting efficient alkaline seawater oxygen evolution reaction of iron oxide hydroxide via plasma-induced oxygen defect engineering

Xiaoqian Du[a], Junjun Zhang*[a], Xuanyu Zhou[a], Mengyuan Zhang[b], Nailiang Wang[a], Xiu Lin[c], Pengfei Zhang*[a,b], Zhenghong Luo [a, b]

[a]State Key Laboratory of High-Efficiency Utilization of Coal and Green Chemical Engineering. College of Chemistry and Chemical Engineering, Ningxia University, Yinchuan, Ningxia, 750021, China. E-mail: zhangjj089@nxu.edu.cn; pfzhang@nxu.edu.cn
[b]School of Chemistry and Chemical Engineering, Shanghai Jiao Tong University, Shanghai, 200240, P. R. China. E-mail:chemistryzpf@sjtu.edu.cn
[c]School of Materials Science and Engineering, Nanyang Technological University, 639798, Singapore.

List of Contents

1. Experiment Section

1.1 Materials

$FeCl_3$ (Aladdin, ≥ 98%), NaCl (Adamas, ≥ 99.9%), RuO_2 (Macklin, ≥ 99.9%), anhydrous ethanol (99.9%), hydrochloric acid (37%), deionized water. All chemicals were used as received without further purification.

1.2 Preparation of FeOOH/SS electrode

In the first place, stainless steel mesh (SS) underwent an initial cleaning with an HCl solution using ultrasound for 20 minutes. It is followed by multiple rinses with ethanol and water to eliminate contaminants and achieve cleanliness. NaCl (20 mmol) and $FeCl_3$(5 mmol) were added to water (50 mL) until it boiled. After that, pre-prepared SS was soaked in the heated solution (60 s). The obtained FeOOH/SS was cleaned using ethanol and allowed to dry at 60℃. The catalyst was loaded at 0.28 mg/cm^2. Furthermore, a range of FeOOH/SS-X s (x=30, 90) catalyst was produced.

1.3 Preparation of P-FeOOH/SS electrode

The obtained FeOOH/SS electrode was transferred to a plasma device (CRF-VPO-2L, Sing Fung, Shenzhen, China), and processed in an Ar plasma atmosphere with 150 W power and at 10 sccm for 4 min. In addition, a range of FeOOH/SS-X min (x=2, 6) catalyst was also produced.

1.4 Preparation of RuO_2/SS electrode

For the preparation of RuO_2-loaded electrodes, 2.8 mg of RuO_2 and 40 μL of 5 wt% Nafion solution were combined in 960 μL of a 1:2 water and ethanol mixture. The mixture underwent ultrasonication for approximately 40 min to create consistent ink. Afterward, 100 μL catalyst ink was applied to a pre-processed SS (1 cm^2).

1.5 Electrochemical characterizations

Electrochemical performance tests were performed at room temperature using an electrochemical workstation (DH7000C, Donghua, Jiangsu, China). P-FeOOH/SS, FeOOH/SS, and RuO_2 were uniformly coated on stainless steel mesh as working electrode, graphite rod and standard Hg/HgO electrode as counter electrode and reference electrode, 1.0 M KOH+ 0.5 M NaCl as electrolyte. At the beginning of the experiment, the catalyst was subjected to 20 cycles of cyclic voltammetry (CV) at 10 mV/s at 0.5-1.2 V to stabilize the catalyst surface. The oxygen evolution performance of the catalyst was determined by linear sweep voltammetry (LSV) in the range of 0 - 1.2 V vs. Hg/HgO. Double layer capacitance (C_{dl}) measurements were conducted by varying the scan rates (20, 40, 60, 80, 100 mV/s) in a potential window nearly without a Faradaic process. The

polarization curves were established as overpotential vs log current (log j) to get Tafel plots for evaluating the OER reaction kinetics of obtained catalysts. By fitting the Tafel plots (the linear portion) to the Tafel equation ($\eta = b\log(j) + a$), the Tafel slope can be obtained. The electrochemical impedance spectroscopy (EIS) test was performed in the frequency range of 0.1-1000 Hz, and the in-situ impedance of the catalyst was measured using EIS in the range of 0.40-0.80 V. In the range of 0.5-1.2 V, 500 CV cycles were carried out at a scan rate of 50 mV s^{-1}. The stability of the catalyst was evaluated by comparing the LVS and EIS before and after 500 CV cycles. The long-term stability of the catalyst was tested at 50 mA cm^{-2}. At the same time, multi-step currents 20, 40, 60, 80, and 100 mA cm^{-2} and multi-step potential 0.6, 0.65, 0.7, 0.75, and 0.8 V were used to evaluate the stability of the catalyst in the dynamic current and potential.

1.6 Material characterizations

The X-ray diffraction (XRD) patterns were recorded on a Rigaku MiniFlex 600-C X-ray diffractometer with Cu-Kα radiation with a scan rate of 5° min^{-1}. The electron paramagnetic resonance (EPR) spectra were collected on a Bruker A300 Paramagnetic spectrometer, which was performed at room temperature in a vacuum. The Raman measurement was performed with a Raman JY HR800 Spectrometer, wavenumber region 150-600 cm^{-1}. The Scanning electron microscopy (SEM) characterizations were conducted using a JSM-7800F from JEOL. Transmission electron microscopy (TEM) and high-resolution transmission electron microscopy (HRTEM) measurements were taken with a JEOL JEM-F200 microscope operated. The X-ray photoelectron spectroscopy (XPS) measurements were conducted on a Kratos Axis Ultra DLD spectrometer. Raman measurements were conducted employing a Raman JY HR800 coupled with an in-situ Raman flow cell (EC-Raman, Beijing Scistar Technology, China). Spectrometer within the wavenumber range of 200-1000 cm^{-1}. A 50× long working distance objective (8 mm) was utilized, and the excitation laser, with a wavelength of 532 nm, originated from a He-Ne laser with an approximate power of 6 mW. Calibration of the Raman frequency was achieved using a Si wafer. Data acquisition involved Raman readings at various constant potentials (1.20-1.70 V vs. RHE), with a stabilization period of 20 seconds preceding each measurement. The counter electrode and reference electrode for Raman measurement comprised a carbon rod and Hg/HgO, respectively. 1.0 M KOH+0.5 M NaCl electrolyte solution was utilized. Fe K-edge X-ray absorption spectra (XAS) were collected at the BL14W beamline from the Shanghai Synchrotron Radiation Facility.

1.7 Computational details

All the calculations are performed in the framework of the density functional theory with the projector-augmented plane-wave method, as implemented in the Vienna ab initio simulation package [1]. The generalized gradient approximation proposed by Perdew, Burke, and Ernzerhof is selected for the exchange-correlation potential [2]. The cut-off energy for the plane wave is set to 520 eV. The energy criterion is set to 10^{-4} eV in the iterative solution of the Kohn-Sham equation. The Brillouin zone integration is performed using a 2×2×8 k-mesh. All the structures are relaxed until the residual forces on the atoms have declined to less than 0.02 eV/Å.

2. Supplementary Figures

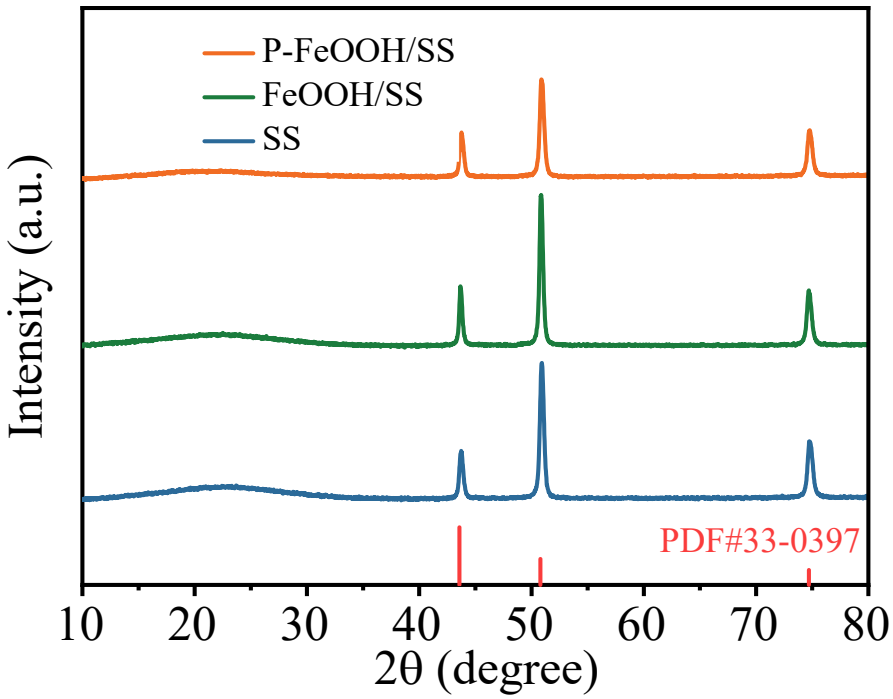

Figure S1. XRD patterns of P-FeOOH/SS, FeOOH/SS and SS.

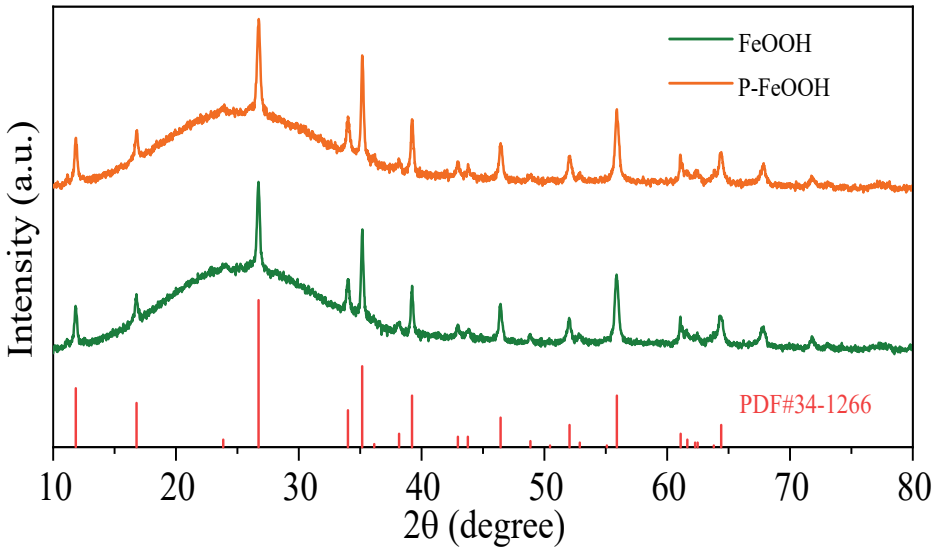

Figure S2. XRD patterns of P-FeOOH and FeOOH.

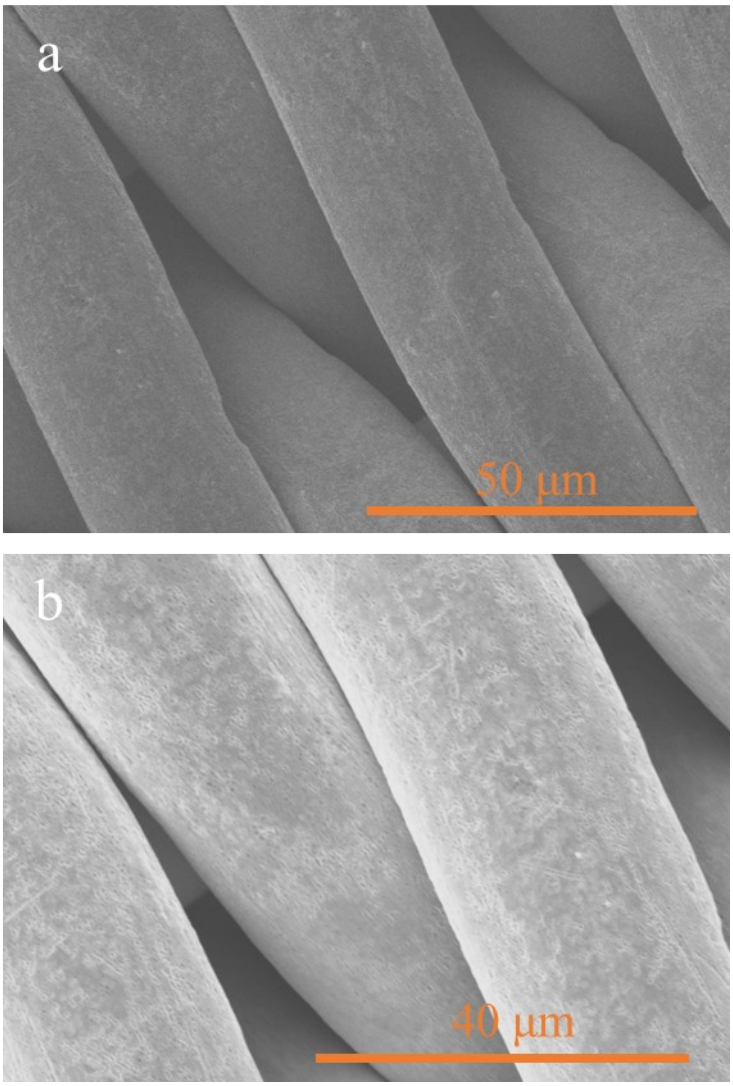

Figure S3. SEM images of P-SS at different magnifications.

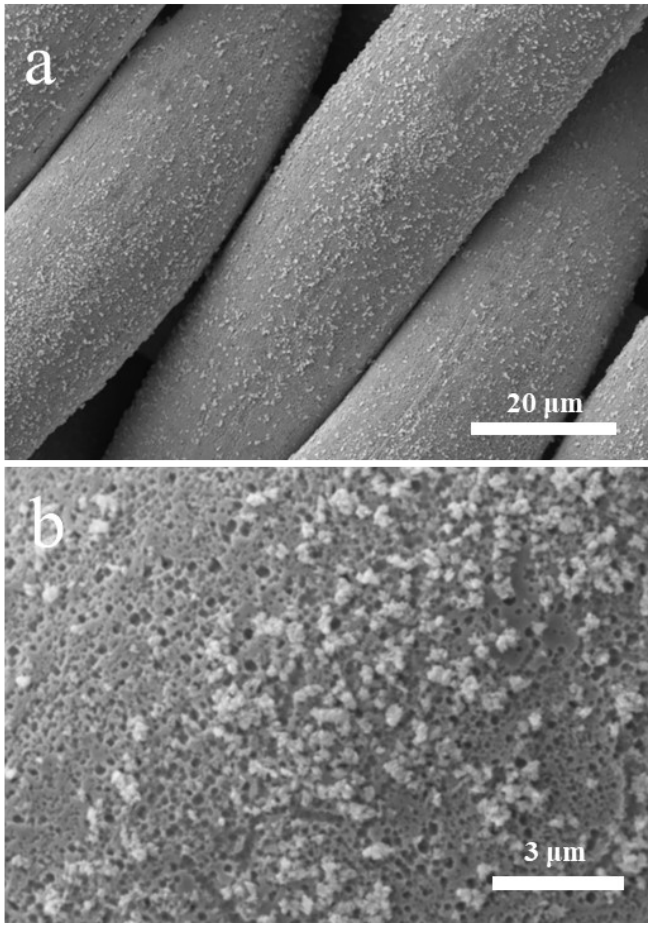

Figure S4. SEM images of P-FeOOH/SS at different magnifications.

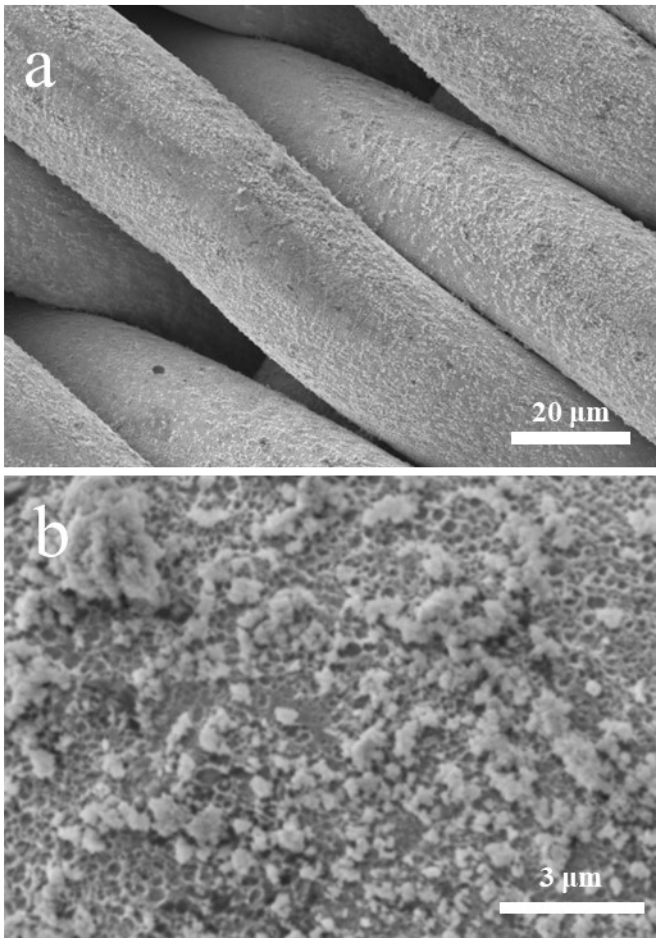

Figure S5. SEM images of FeOOH/SS at different magnifications.

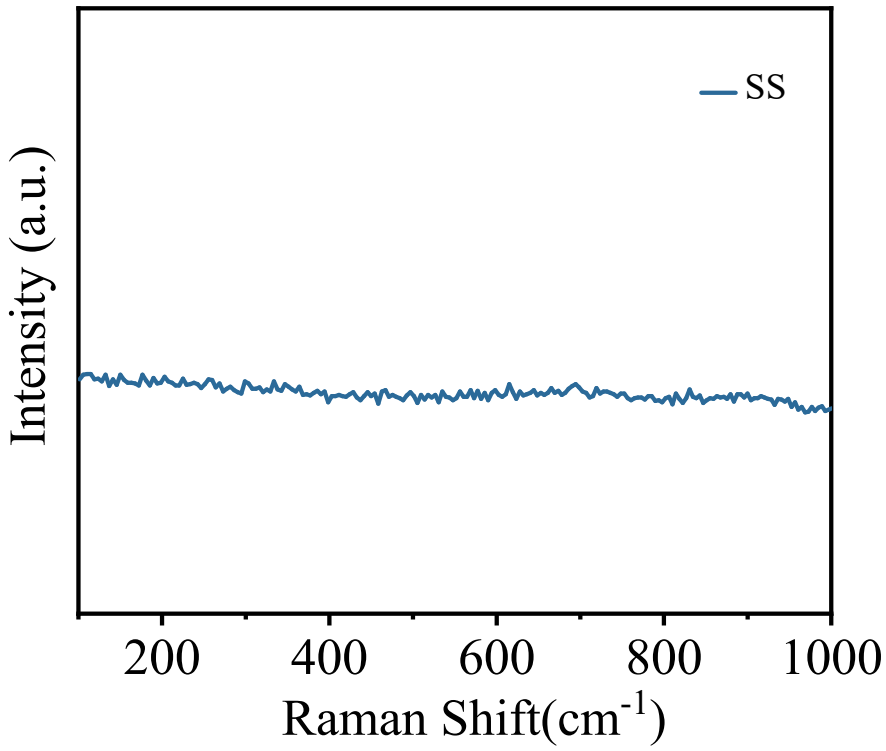

Figure S6. The Raman spectrum of SS.

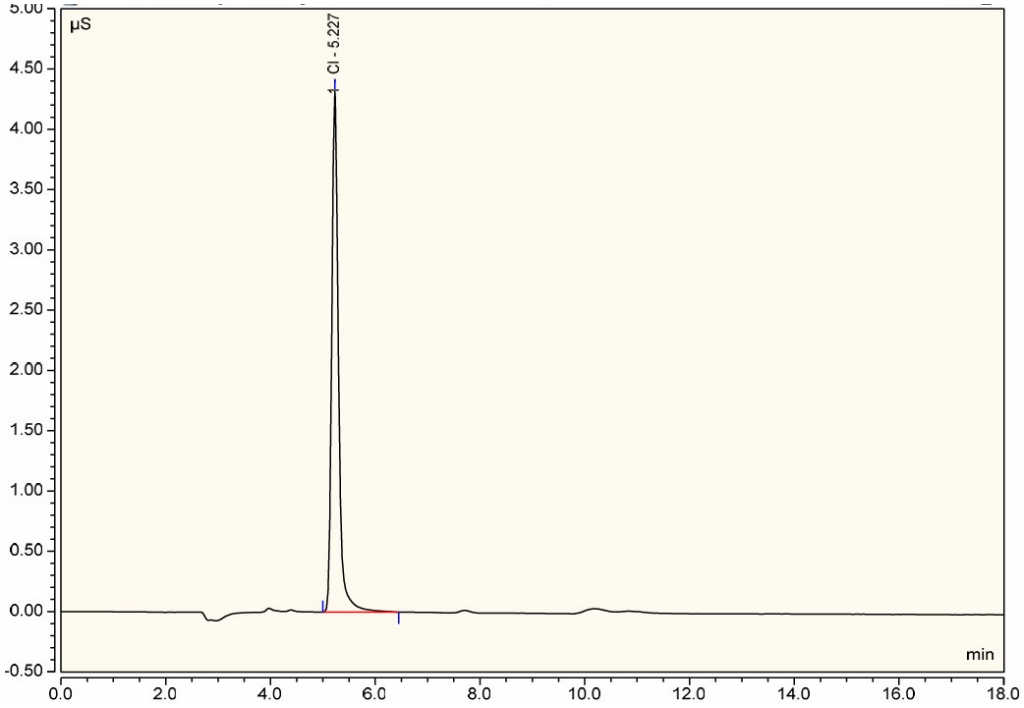

Figure S7. Ion chromatographic analysis of Cl content in catalysts.

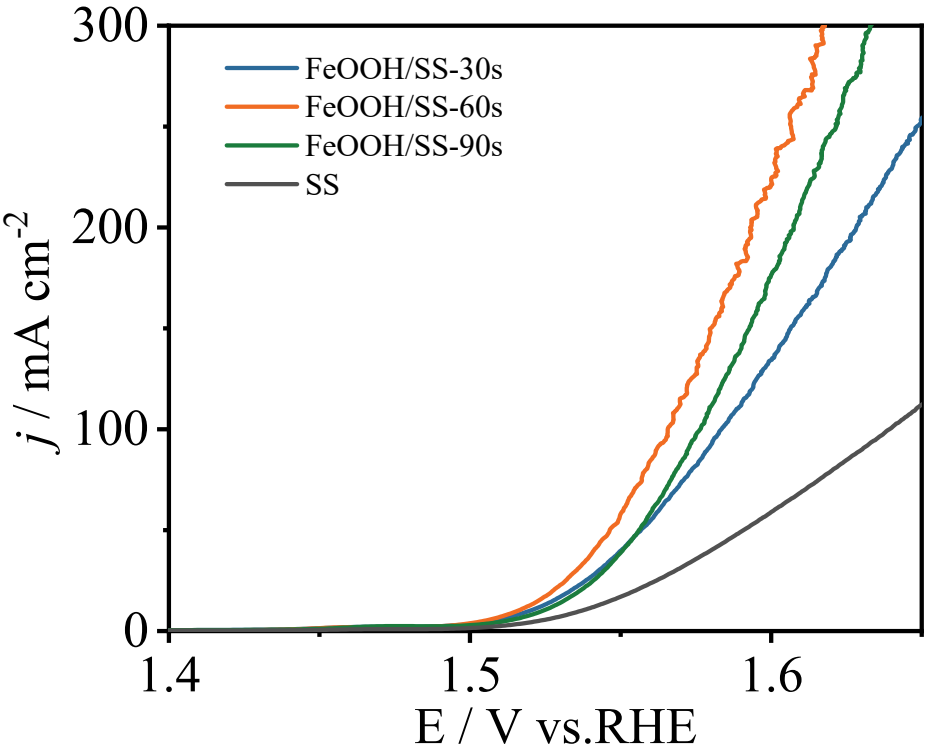

Figure S8. Optimized LSV curves of samples at different reaction times.

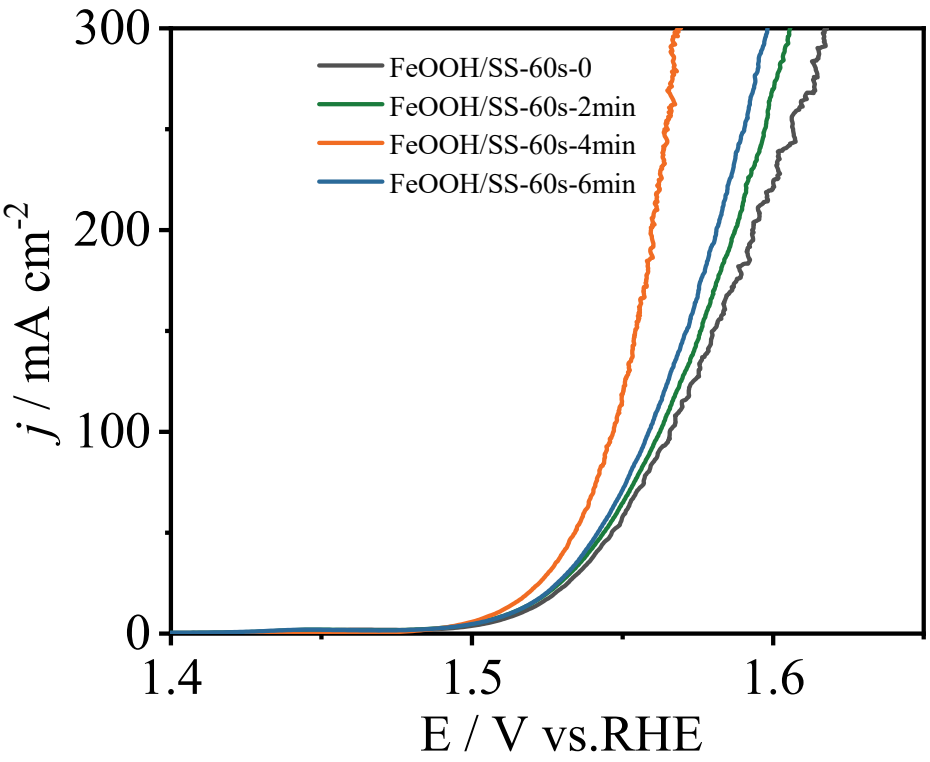

Figure S9. Optimized LSV curves of samples in different plasma treatment times.

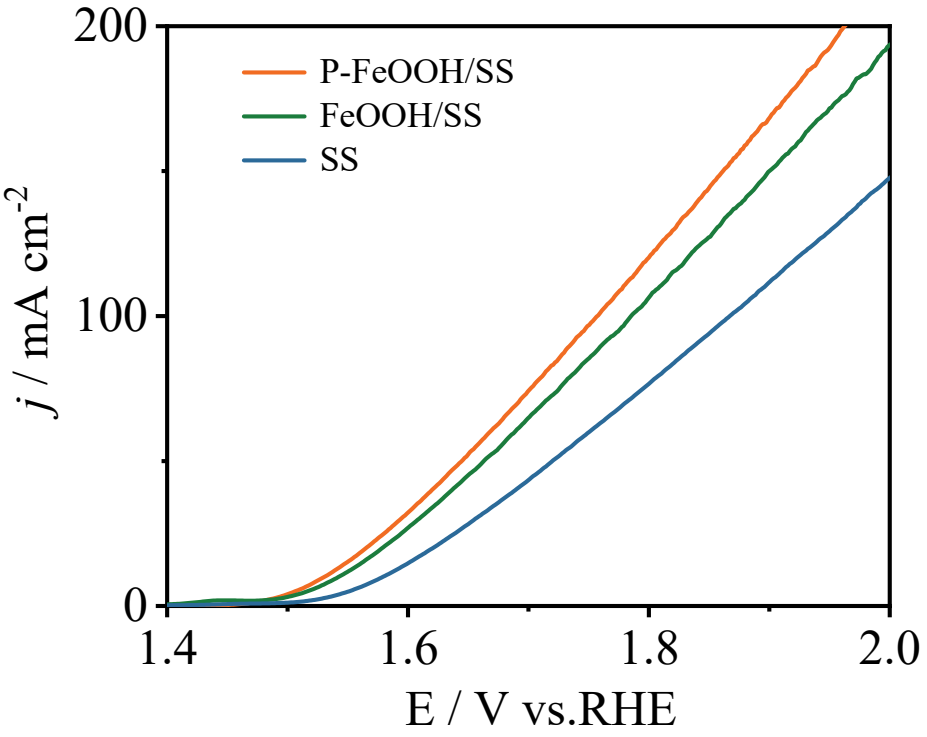

Figure S10. LSV graph without i-R correction.

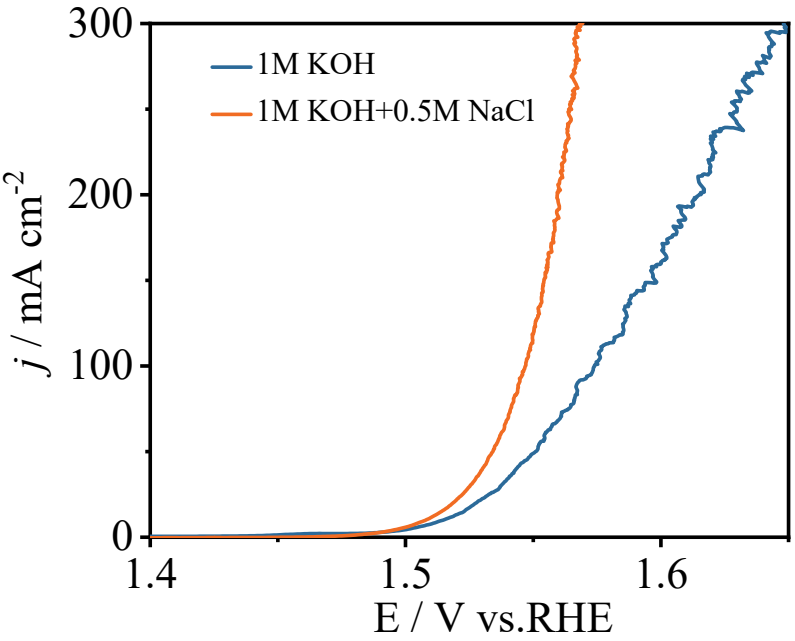

Figure S11. Comparison of LSV curves of P-FeOOH/SS in alkaline seawater and alkaline solutions.

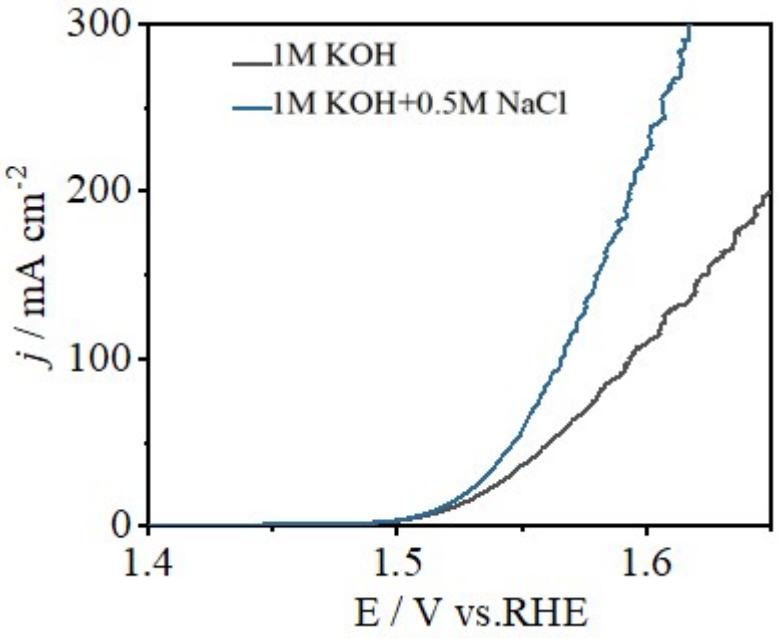

Figure S12. Comparison of LSV curves of FeOOH/SS in alkaline seawater and alkaline solutions.

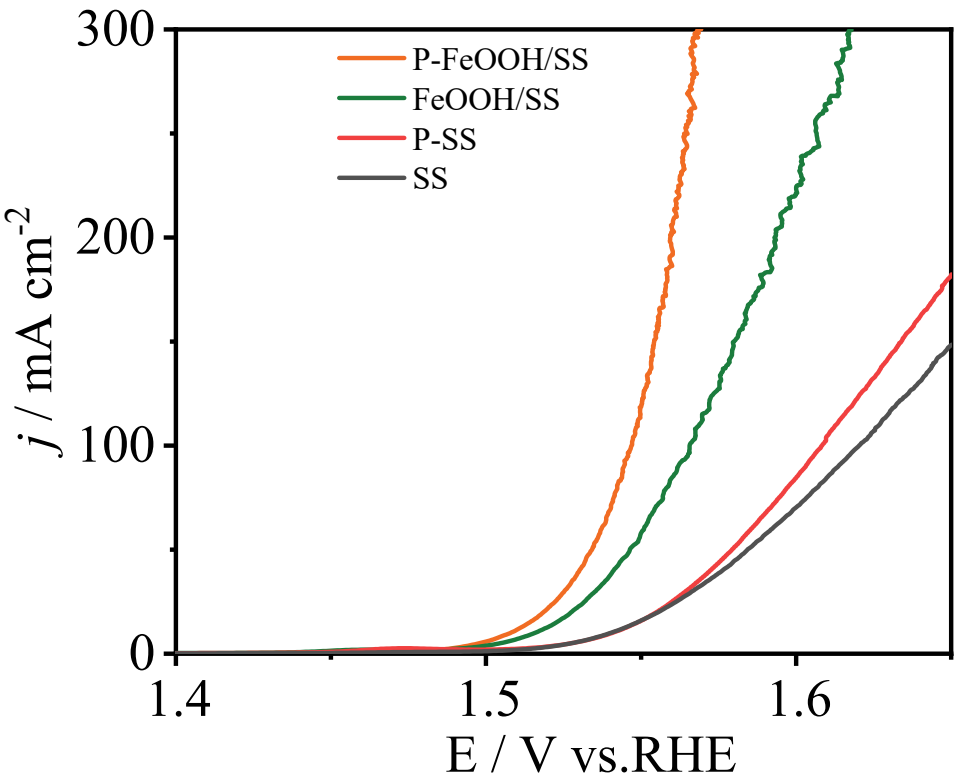

Figure S13. LSV curves for P-FeOOH/SS, FeOOH/SS, P-SS and SS electrodes in 1.0 M KOH+0.5 M NaCl electrolyte.

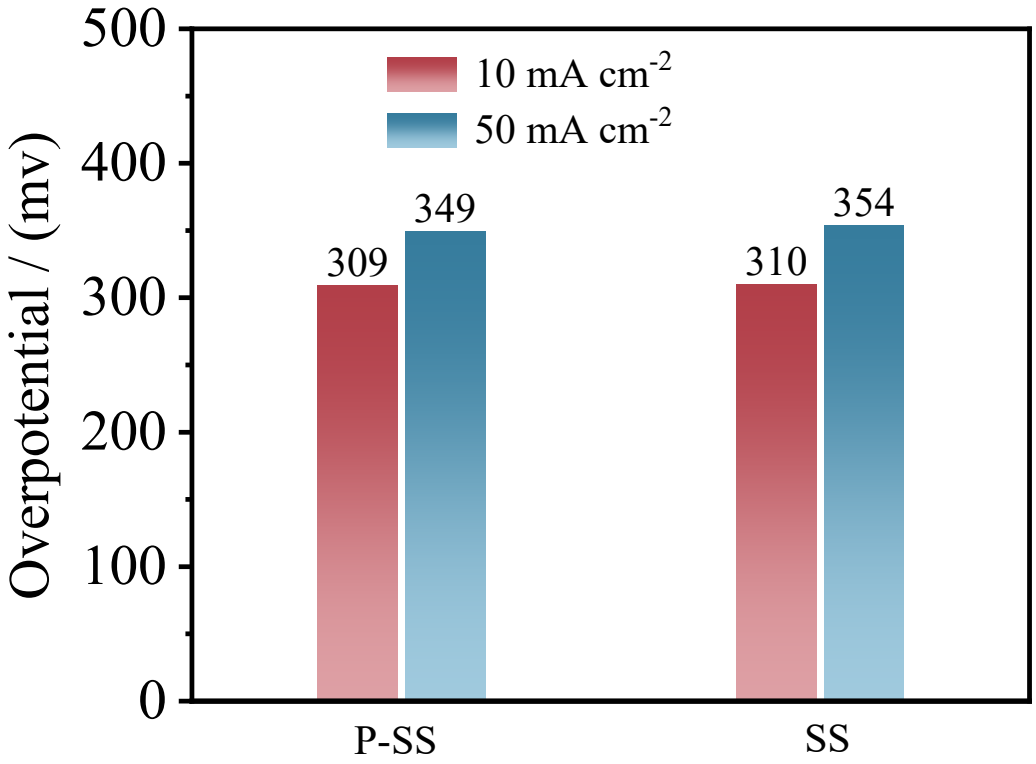

Figure S14. The comparison of overpotential at 10 and 50 mA cm^{-2} for P-SS and SS electrodes in 1.0 M KOH+0.5 M NaCl electrolyte.

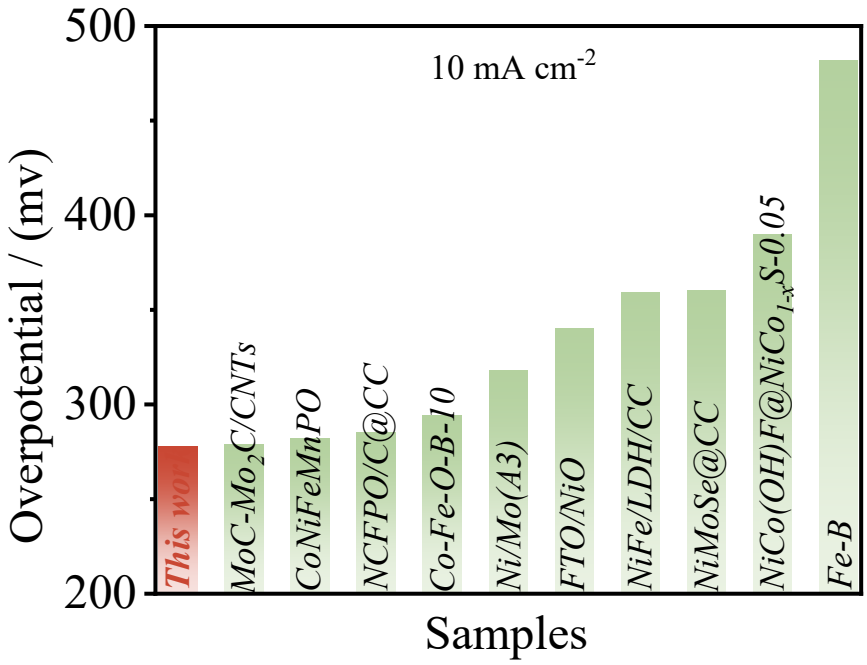

Figure S15. Performance comparison of P-FeOOH/SS with reported excellent catalysts in 1.0 M KOH+0.5 M NaCl electrolyte.

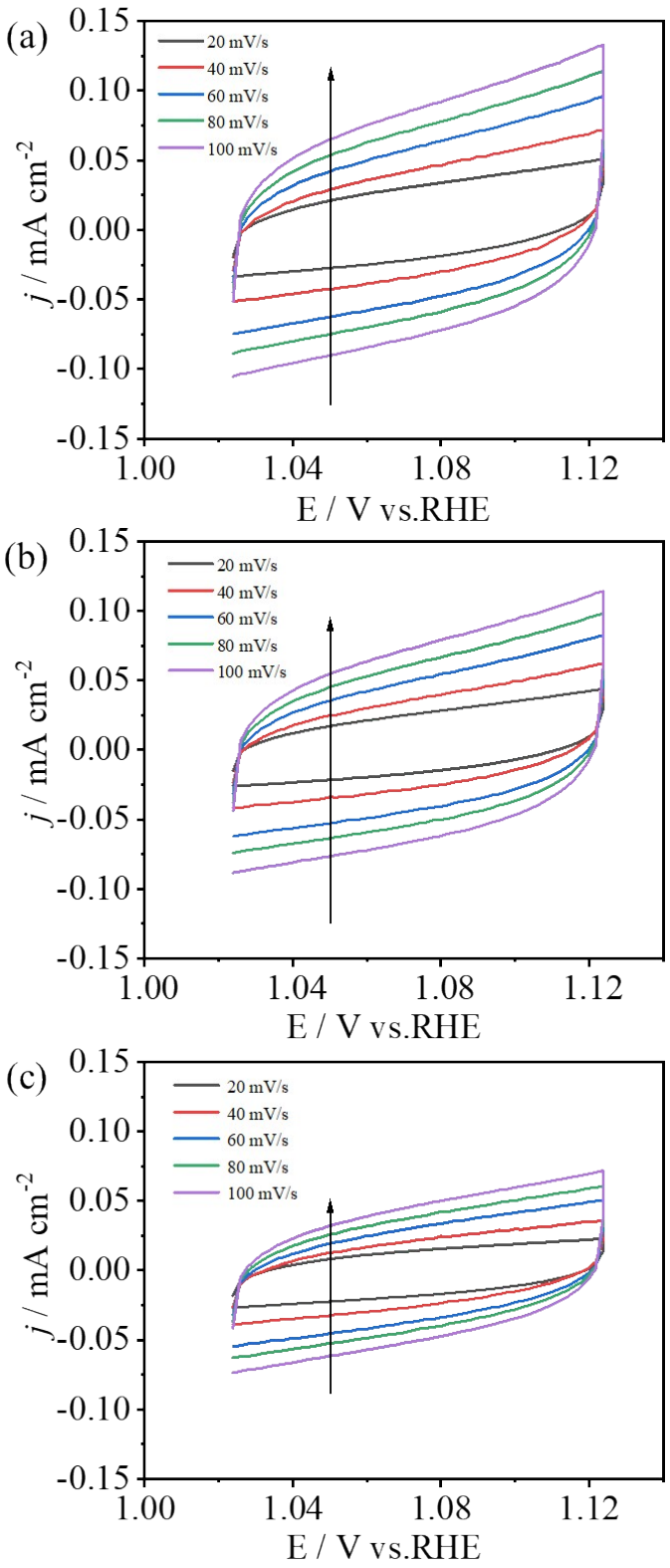

Figure S16. CV curves of (a) P-FeOOH/SS (b) FeOOH/SS (c) SS electrodes at different scan rates from 20 to 100 mV s^{-1}.

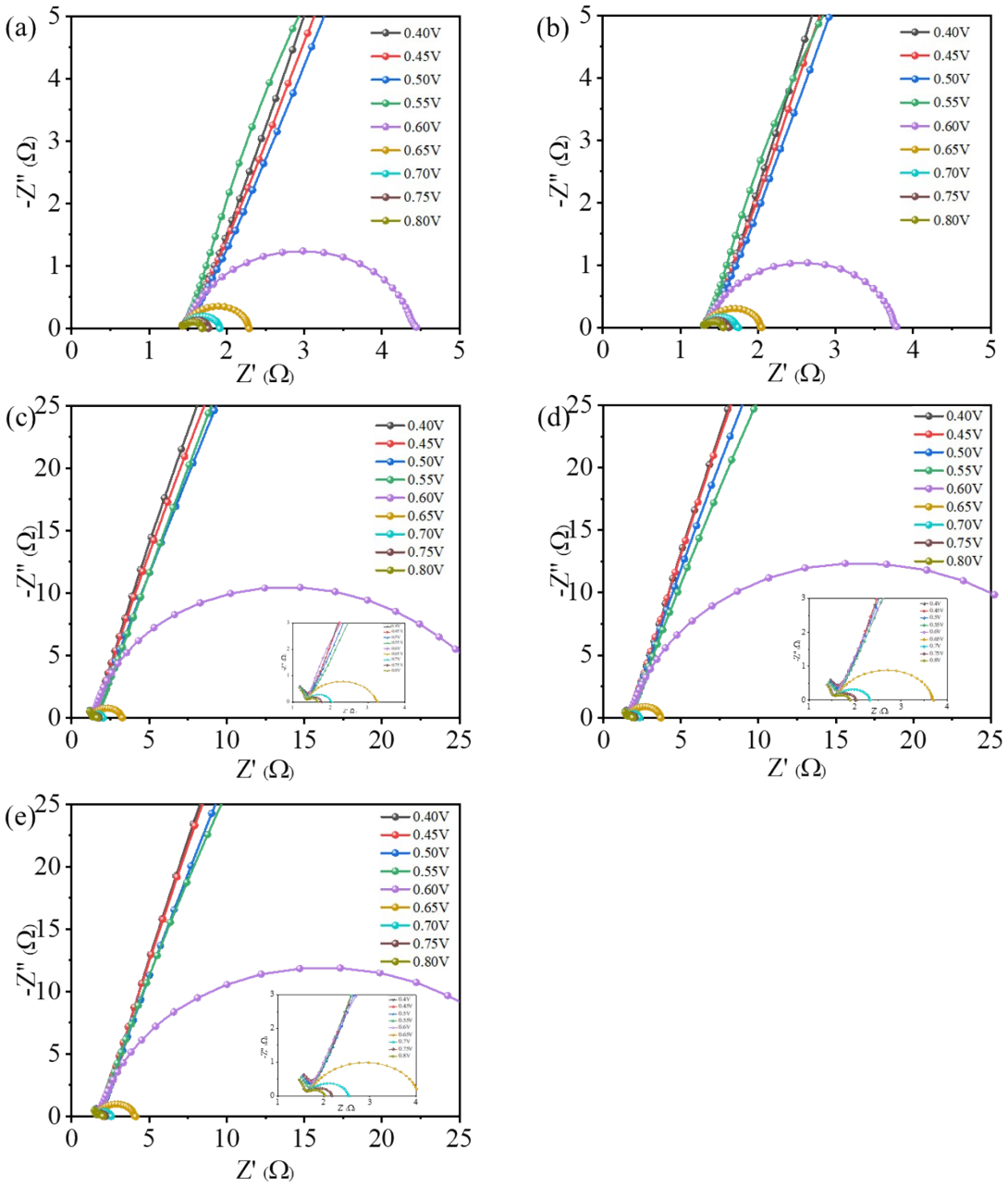

Figure S17. Operando Nyquist plots of the samples at various potentials. (a)P-FeOOH/SS, (c) FeOOH/SS and (e) SS in 1M KOH. (b) FeOOH/SS and (d) SS in 1.0 M KOH+0.5 M NaCl.

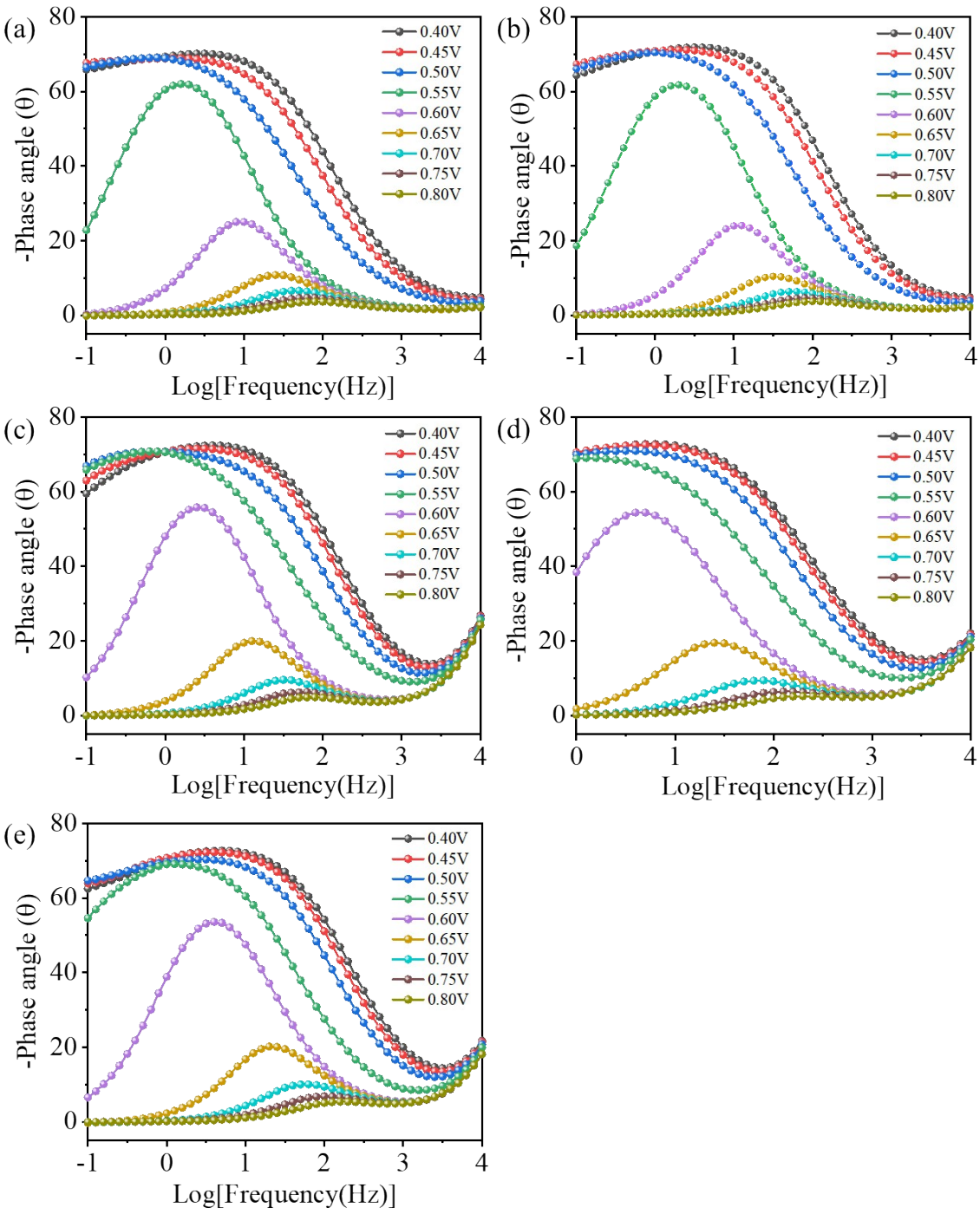

Figure S18. Bode phase plots of the samples at various potentials. (a)P-FeOOH/SS, (c) FeOOH/SS and (e) SS in 1.0 M KOH. (b) FeOOH/SS and (d) SS in 1.0 M KOH+0.5 M NaCl.

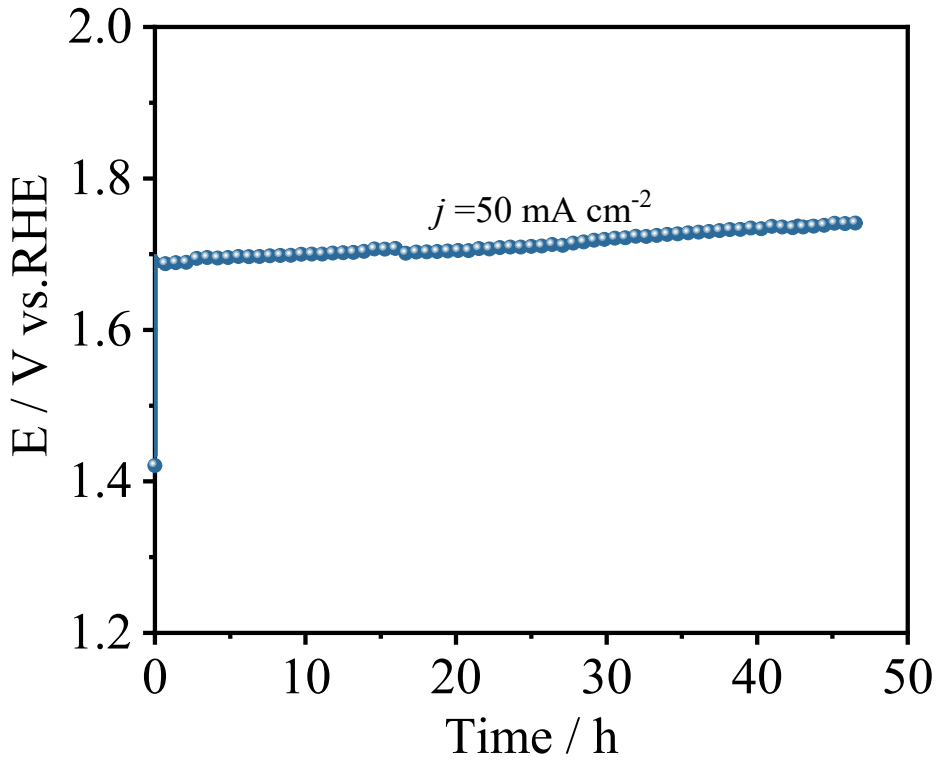

Figure S19. The long-time E-t curve of the P-FeOOH/SS in 1.0 M KOH for OER (j=50 mA cm^{-2}).

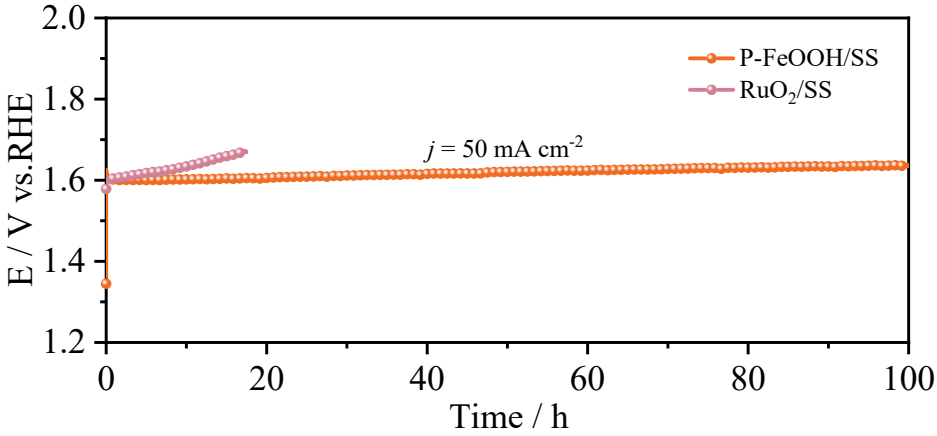

Figure S20. The long-time E-t curves of the P-FeOOH/SS and RuO_2/SS in 1.0 M KOH+0.5 M NaCl for OER (j=50 mA cm^{-2}).

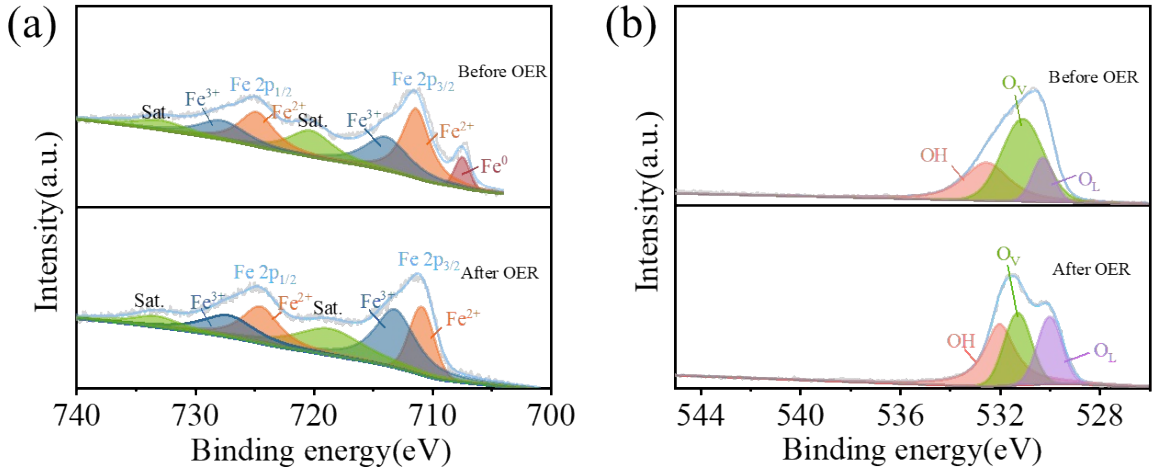

Figure S21. (a) Fe 2p and (b) O 1s XPS spectra of P-FeOOH/SS before and after OER.

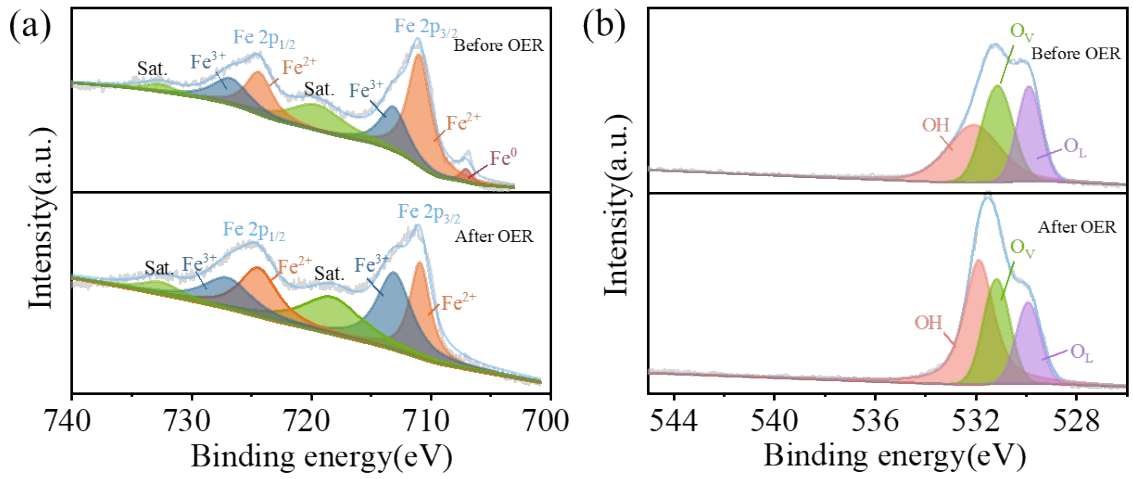

Figure S22. (a) Fe 2p and (b) O 1s XPS spectra of FeOOH/SS before and after OER.

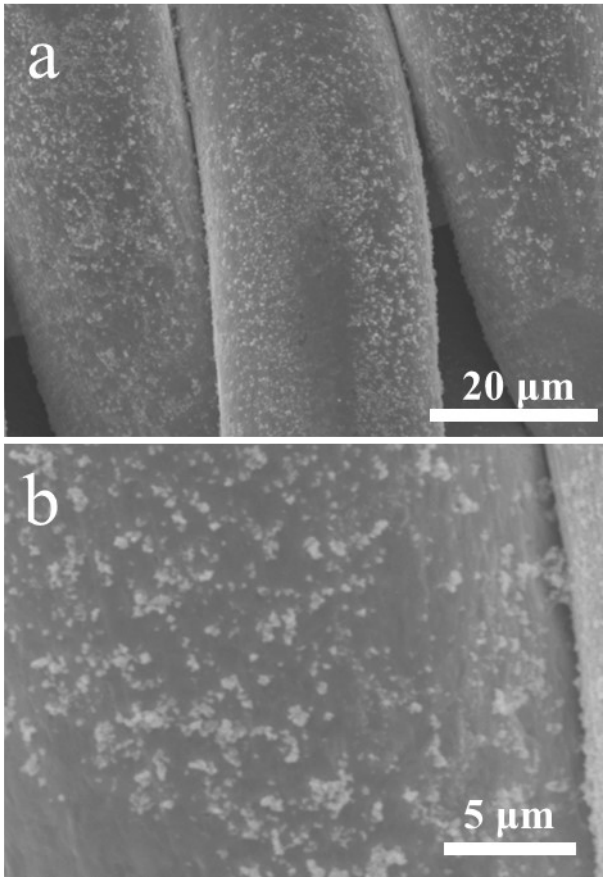

Figure S23. SEM images of P-FeOOH/SS after OER at different magnifications.

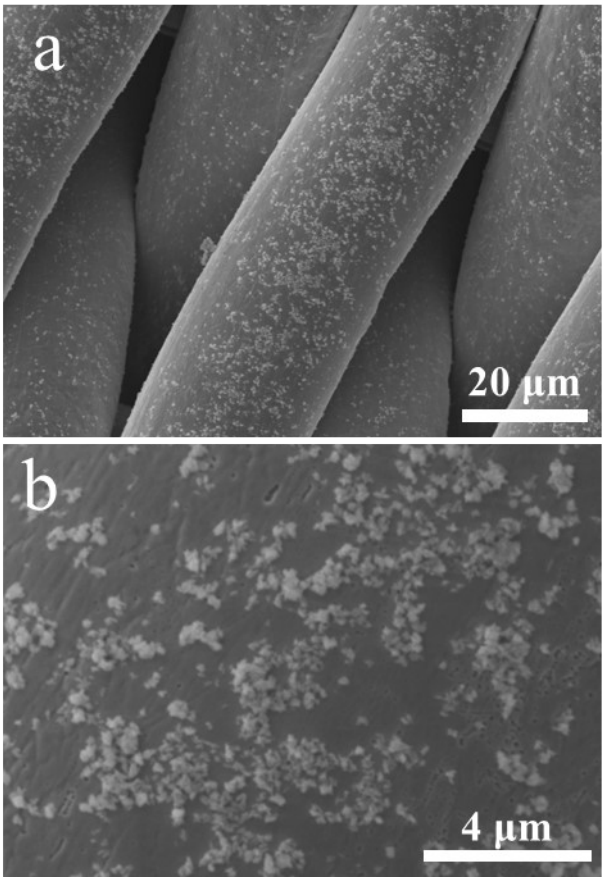

Figure S24. SEM images of FeOOH/SS after OER at different magnifications.

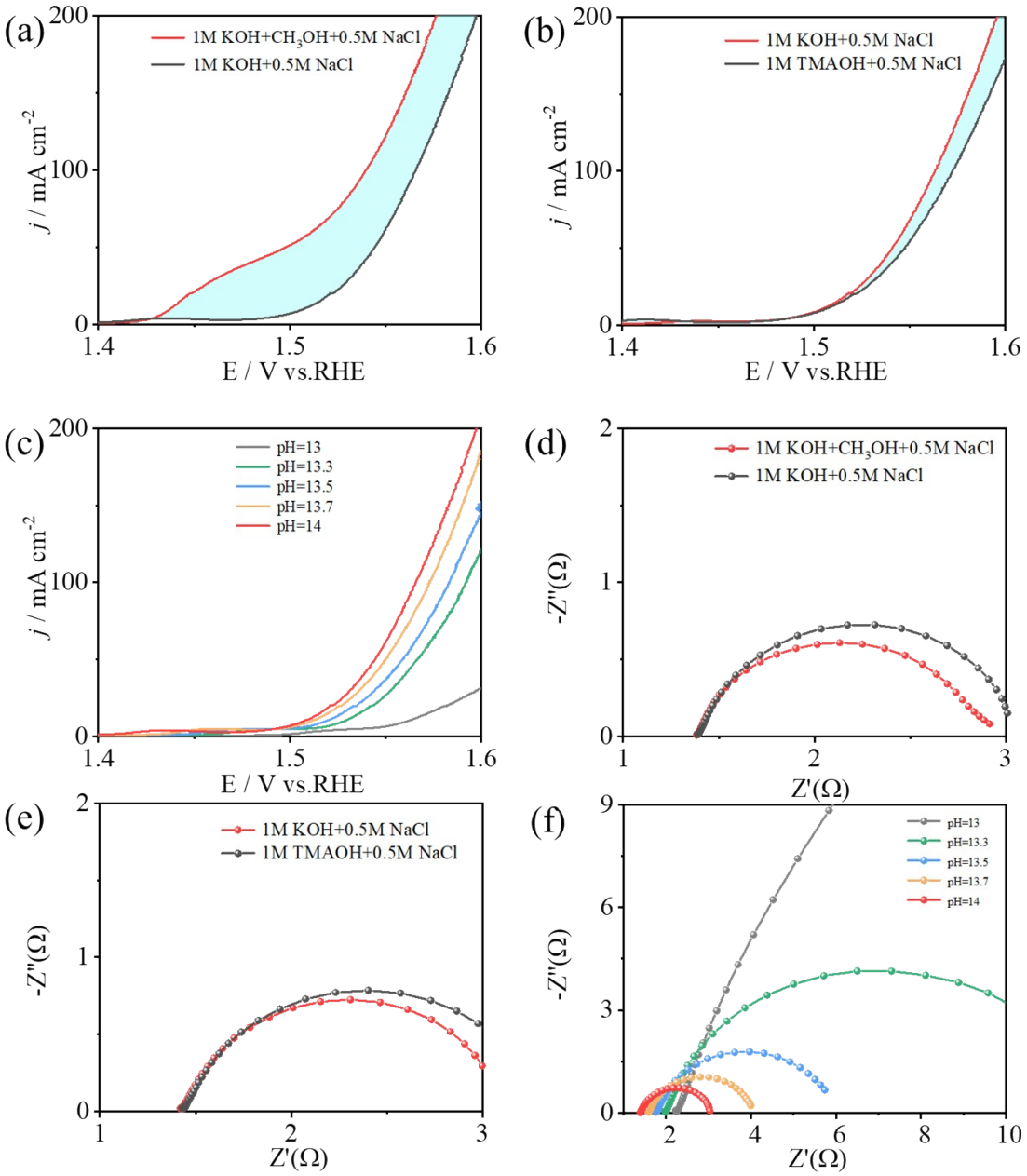

Figure S25. (a) LSV curves and (d) EIS plots of FeOOH/SS in 1.0 M KOH+0.5 M NaCl (with and without methanol). (b) LSV curves and (e) EIS plots of FeOOH/SS in 1.0 M KOH+0.5 M NaCl and 1.0 M TMAOH+0.5 M NaCl. (c) LSV curves and (f) EIS plots of FeOOH/SS in electrolytes with different pH values.

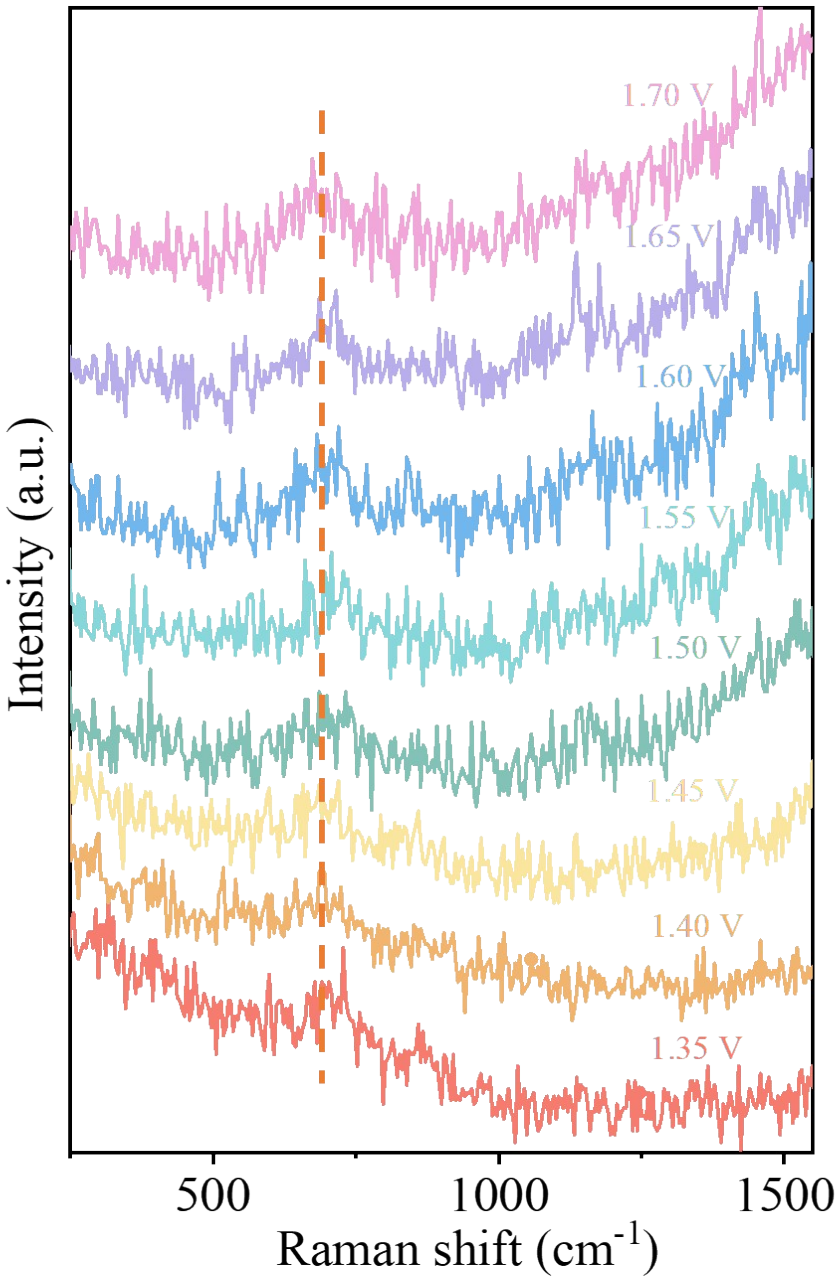

Figure S26. In-situ Raman plots of FeOOH/SS.

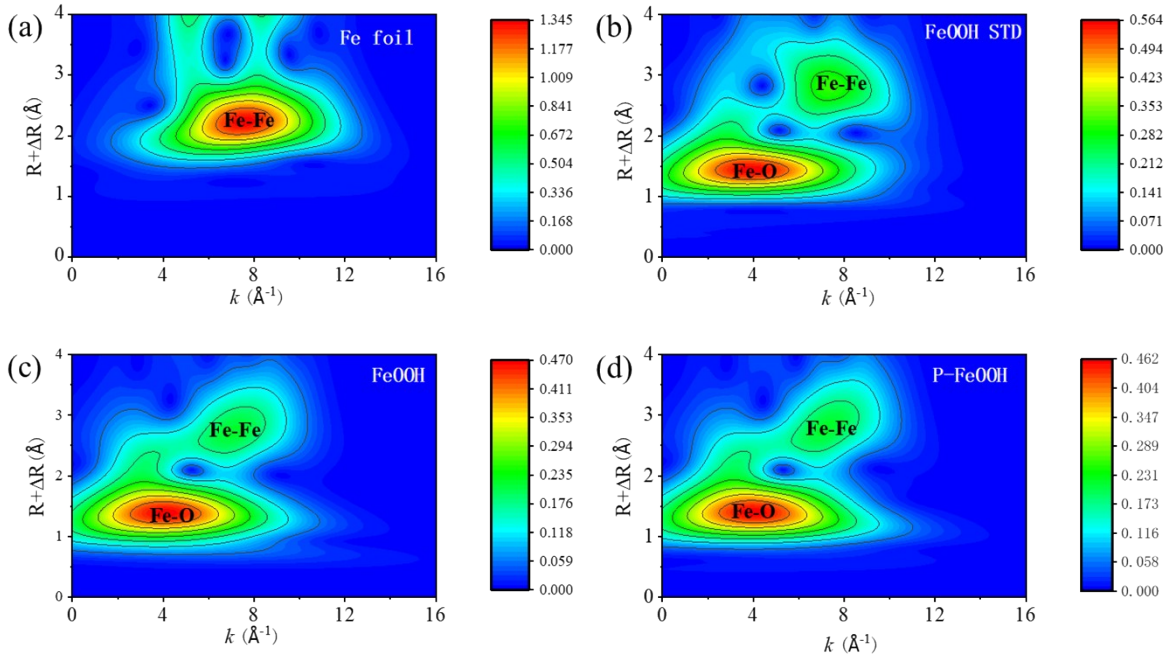

Figure S27. Wavelet transforms EXAFS of (a) Fe foil, (b) FeOOH STD, (c) FeOOH, and (d) P-FeOOH.

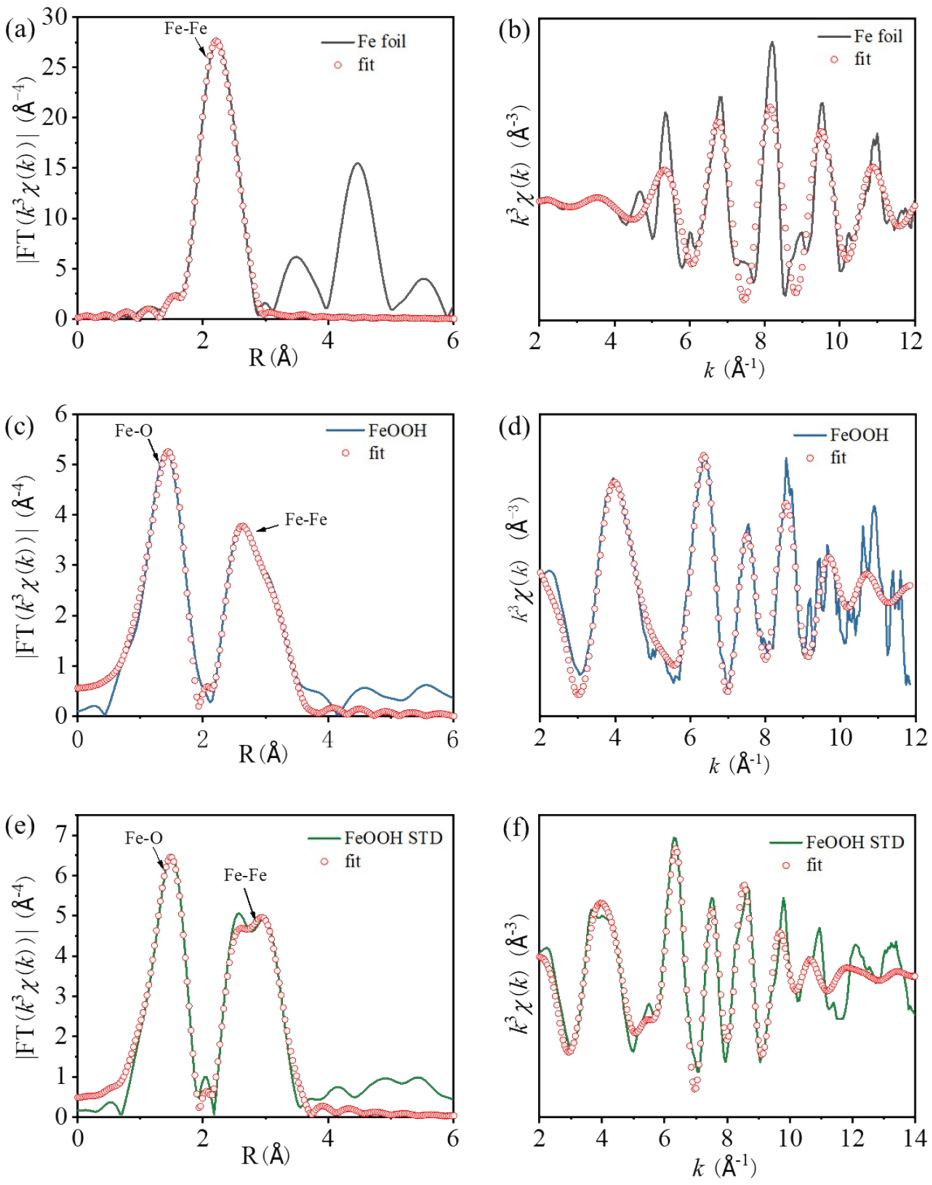

Figure S28. Fe K-edge EXAFS oscillation function $k^3\chi$ (k) and FT plots of the EXAFS $k^3\chi$ (k) function in R-space of different samples: (a-b) Fe foil, (c-d) FeOOH and (e-f) FeOOH STD.

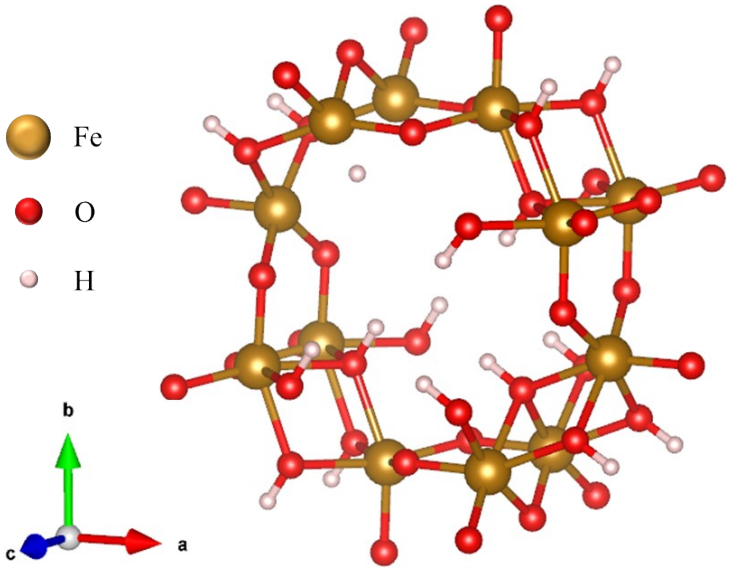

Figure S29. Optimized structural models of P-FeOOH.

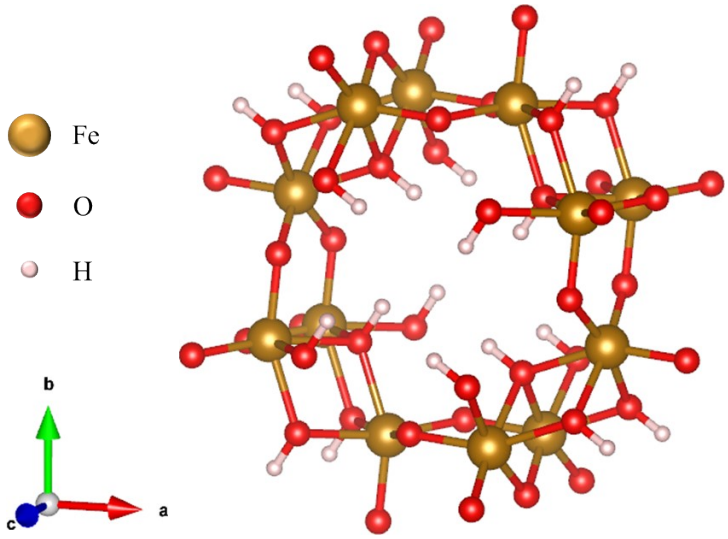

Figure S30. Optimized structural models of FeOOH.

3. Supplementary Tables

Table S1. EXAFS data fitting results of Samples.

Sample	Path	*CN*[a]	*R*(Å)[b]	σ^2 (Å^2)[c]	ΔE_0(eV)[d]	*R* factor	*Range of k*	*Range of R*
Fe K-edge (S_0^2=0.745)								
Fe foil	Fe-Fe	8.0*	2.464	0.0057	4.9	0.0028	2-11.8	1-3
	Fe-Fe	6.0*	2.839					
FeOOH-STD	Fe-O	6.2	1.997	0.0116	-3.9	0.0156	2-10	1-3.5
	Fe-Fe	5.5	3.043	0.0122	-1.6			
	Fe-Fe	6.3	3.442		4.1			
FeOOH	Fe-O	5.5	1.978	0.0156	-4.9	0.01169	2-10	1-3.5
	Fe-Fe	4.2	3.067	0.0135	3.2			
	Fe-Fe	2.9	3.464		8.8			
P-FeOOH	Fe-O	5.6	1.984	0.0180	-4.2	0.0196	2-10	1-3.5
	Fe-Fe	3.8	3.096	0.0171	5.6			
	Fe-Fe	3.7	3.473		9.9			

[a]*CN*, coordination number; [b]*R*, the distance between absorber and backscatter atoms; [c]σ^2, the Debye Waller factor value; [d]ΔE_0, inner potential correction to account for the difference in the inner potential between the sample and the reference compound; *R* factor indicates the goodness of the fit. S_0^2 was fixed to 0.745, according to the experimental EXAFS fit of Fe foil by fixing *CN* as the known crystallographic value. * This value was fixed during EXAFS fitting, based on the known structure of Fe. Fitting space: R space; *k*-weight = 3. A reasonable range of EXAFS fitting parameters: 0.700 < S_0^2 < 1.000; *CN* > 0; σ^2 > 0 Å^2; $|\Delta E_0|$ < 15 eV; *R* factor < 0.02.

Table S2. Comparison of OER performance in 1.0 M KOH+0.5 M NaCl for the as-prepared catalysts in this study with the other reported catalysts in literature.

Catalysts	η_{10} (mV)	Condition	Reference
P-FeOOH/SS	278	1M KOH+0.5M NaCl	This work
MoC-Mo_2C/CNTs	279	1M KOH+0.5M NaCl	[3]
CoNiFeMnPO	282	1M KOH+0.5M NaCl	[4]
NCFPO/C@CC	285	1M KOH+0.5M NaCl	[5]
Co-Fe-O-B-10	294	1M KOH+0.5M NaCl	[6]
Ni/Mo(A3)	318	1M KOH+0.5M NaCl	[7]
FTO/NiO	340	1M KOH+0.5M NaCl	[8]
NiFe/LDH/CC	359	1M KOH+0.5M NaCl	[9]
NiMoSe@CC	360	1M KOH+0.5M NaCl	[10]
NiCo(OH)F@$NiCo_{1-x}S$-0.05	390	1M KOH+0.5M NaCl	[11]
Fe-B	482	1M KOH+0.5M NaCl	[12]
NiMn/Ti-1	386	1M KOH+0.5M NaCl	[13]
$Co(OH)_3Cl$	379	1M KOH+0.6M NaCl	[14]
ER-RP/P-SNCF-5	332	1M KOH+0.5M NaCl	[15]
oct_Cu_2O-NF	354	1M KOH+0.5M NaCl	[16]
Co-CoO@C (denoted as ZIF67-600Ar/GF)	374	1M KOH + Seawater	[17]
CoSe/$MoSe_2$/NF	350	1M KOH + Seawater	[18]
$Ni_{12}P_5$/FeOOH/NF	235(η_{100}) 327(η_{100})	1M KOH 1M KOH + Seawater	[19]

4. References

1 G. Kresse, D. Joubert, *Phys. Rev. B,* 1999, **59**, 1758.

2 J.P. Perdew, K. Burke, M. Ernzerhof, *Phys. Rev. Lett.*,1996, **77**, 3865.

3 J.Q. Wang, T.H. Nguyen, K.X. Dong, D.T. Tran, N.H. Kim, J.H. Lee, *Int. J. Hydrogen Energy,* 2024, **49**, 1005-1013.

4 H.M. Zhang, L.H. Zuo, Y.H. Gao, J.X. Guo, C.Z. Zhu, J. Xu, J.F. Sun, *J. Mater. Sci. Technol.*, 2024, **173**, 1-10.

5 H.J. Song, H. Yoon, B. Ju, D.Y. Lee, D.W Kim, *ACS Catal.*, 2019, **10**, 702-709.

6 S. Gupta, M. Forster, A. Yadav, A.J. Cowan, N. Patel, M. Patel, *ACS Appl. Energy Mater.,* 2020, **3**, 7619-7628.

7 W.J. Yuan, Z.D. Cui, S.L. Zhu, Z.Y. Li, S.L. Wu, Y.Q. Liang, *Electrochim. Acta*, 2021, **365**, 137366.

8 J. Juodkazytė, B. Šebeka, I. Savickaja, M. Petrulevičienė, S. Butkutė, V. Jasulaitienė, A. Selskis, R. Ramanauskas, *Int. J. Hydrogen Energy*, 2019, **44**, 5929-5939.

9 F. Dionigi, T. Reier, Z. Pawolek, M. Gliech, P. Strasser, *ChemSusChem*, 2016, **9**, 962-972.

10 M. Saquib, P. Arora, A.C. Bhosale, *Fuel*, 2024, **365**, 131251.

11 S.N. Na, D.F. Chai, J.L. Li, S.J. Chen, X. Yang, S.S. Fu, G.Z. Sui, D.X. Guo, *J. Colloid Interface Sci.*, 2024, **655**, 145-156.

12 R. Silviya, Y. Vernekar, A. Bhide, S. Gupta, N. Patel, R. Fernandes, *ChemCatChem*, 2023, **15**，e202300635.

13 S. Barua, A. Balčiūnaitė, D. Upskuvienė, J. Vaičiūnienė, L. Tamašauskaitė-Tamašiūnaitė, E. Norkus, *Coatings*, 2024, **14**, 1074.

14 L.Z. Zhuang, J.K. Li, K.Y. Wang, Z.H. Li, M.H. Zhu, Z. Xu, *Adv. Funct. Mater.*, 2022, **32**, 2201127.

15 F.Y. Liu, R.G. Hu, H.Q. Qiu, H. Miao, Q. Wang, J.L. Yuan, *J. Alloys Compd.,* 2022, **913**, 165342.

16 H. Wang, J. Ying, Y.X. Xiao, J.B. Chen, J.H. Li, Z.Z. He, H.J. Yang, X.Y. Yang, *Electrochem. Commun.,* 2022, **134**, 107177.

17 S. Fathima T.K, A. Ghosh, S. Ramaprabhu, *Int. J. Hydrogen Energy*, 2024, **49**,780-793.

18 J.P. Sun, J. Li, Z.Z. Li, C.H. Li, G.M. Ren, Z.S. Zhang, X.C. Meng, *ACS Sustainable Chem. Eng.,* 2022, **10**, 9980-9990.

19 W Yan, Z Shi, H Feng, J Yu, W Chen, Y Chen, *J. Colloid Interface Sci.*, **2024**, 667, 362.